ACS APPLIED POLYMER MATERIALS

pubs.acs.org/acsapm
Article

Substituting Small Molecules by Polymers in Light Harvesting Capacitor: Effect on the Coherency of Photogenerated Dipoles

Joaquim B. de Lima Filho,* Florian Günther, Bruno Bassi Millan Torres, and Paulo B. Miranda

Cite This: ACS Appl. Polym. Mater. 2024, 6, 8040−8047
Read Online

ACCESS | Metrics & More | Article Recommendations

ABSTRACT: We compare optical and electric properties of multilayered light harvesting capacitors (LHCs) fabricated by layer-by-layer (LbL) polyelectrolyte self-assembly. Electron donor nanolayers were coated from a solution of poly(3-potassium-6-hexanoate thiophene) (P3KHT) while electron acceptor layers were coated from a solution of either a small molecule cationic derivative of *N*,*N*′-bis(6-aminohexil)-3,4,9,10-perilenediimide (PDI-6N) or a macromolecule obtained from a polycation of perylenediimide-functionalized polyethileneimine (PDI-PEI). Internal photogeneration of charges was probed via time-resolved transient absorption and continuous-wave photoinduced absorption spectroscopy, while coherent nanodipoles were probed via transient photocurrent measurements, fitted by an analytical equation developed under photophysical principles of LHCs. Data show that charge lifetimes do not depend on external parameters, especially load resistance and pump modulation frequency, while dipole lifetimes depend on load resistance. In addition, it is shown that LHCs based on polymeric acceptor PDI-PEI are more efficient than those based on small molecule acceptor PDI-6N, probably because the smaller acceptor interpenetrates more into the P3KHT polymeric chains, resulting in weaker coherent contribution of photogenerated dipoles to the macroscopic dielectric polarization.

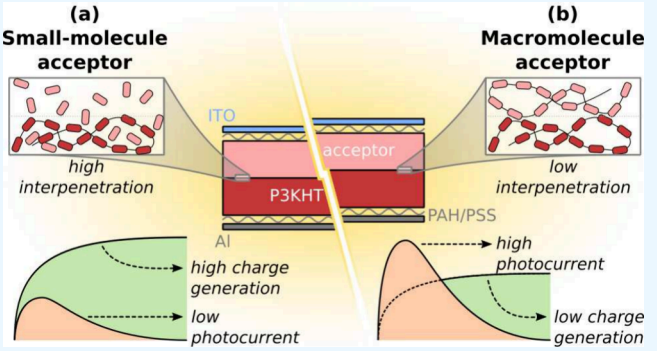

KEYWORDS: *light harvesting capacitor, organic photovoltaics, layer-by-layer assembly, continuous-wave photoinduced absorption, time-resolved transient absorption, photoinduced charge transfer*

1. INTRODUCTION

Energy is an issue for human civilization, and photovoltaic devices promise to play a fundamental role, since sunlight is a limitless renewable source.[1−4] In this sense, the organic electronics research community has focused on organic photovoltaic (OPV) devices due to their unique properties such as low cost and ease of fabrication, absorption tunability, mechanical flexibility, and light weight.[2,5−7] However, one drawback of OPVs is that they present lower power conversion efficiency (PCE) than inorganic photovoltaics (IPVs) mainly due to large losses in the open-circuit voltage and short-circuit current. The latter is mainly due to limitation in charge extraction and significant charge recombination in these low-mobility materials.[3,8]

Aiming to overcome charge extraction issues, Lanzani and his team proposed, in 2012, an OPV architecture, the light harvesting capacitor (LHC),[9] consisting of flat layers of donor and acceptor materials sandwiched between transparent insulating layers and electrodes (Figure 1). In such a device under illumination, generated excitons diffuse and eventually dissociate at the donor−acceptor interface.[10,11] Then, electron and hole follow the built-in electric field caused by the different

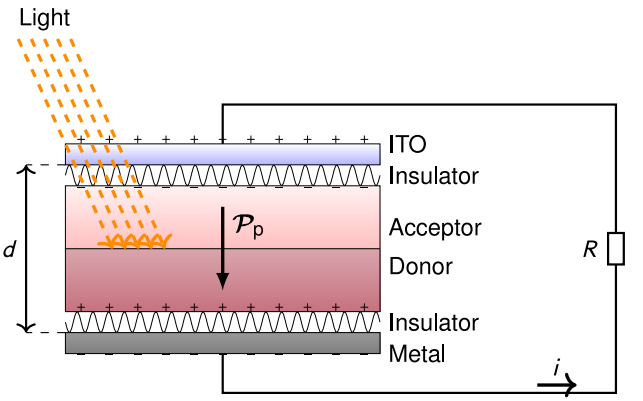

Figure 1. Photoinduced polarization $\mathcal{P}_p$ on an LHC. The waved lines between the active layer (acceptor/donor) and the contacts represent the insulating layers.

Received: March 10, 2024
Revised: June 24, 2024
Accepted: June 25, 2024
Published: July 10, 2024

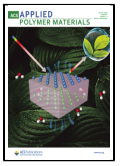

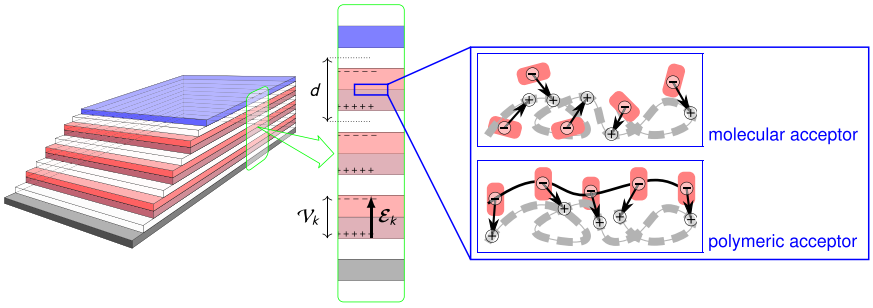

Figure 2. Left: Sketch of a multilayered LHC with metallic contact (gray), insulating layers (white), active layers (red), and a transparent electrode (blue). **Right:** Comparison between interpenetration of donor and acceptor layers when using polymeric donor with molecular acceptor (top) and polymeric acceptor (bottom).

work functions of the electrode materials and migrate in opposite directions.[12] In contrast to solar cells, however, the charges are not extracted at the electrodes but accumulate due to the insulating interfacial layer. Thus, a dipole is generated inside the device, polarizing the active layer, which also acts as a dielectric material of the capacitor formed by the electrodes. This polarization process causes a transient current through the external circuit, until the system reaches equilibrium again. When the illumination ceases, the charges recombine within the donor−acceptor bilayer, and the device generates a reverse transient current.

The efficiency of LHC devices depends on the total polarization obtained in the active layer, which is larger for either a bigger separation of electrons and holes perpendicular to the electrode surfaces (coherent polarization) or more charges being generated. For long lasting illumination, the total separation is limited by the mobility and the lifetime of the charges. Since mobility is quite low in traditional semiconducting organic materials, a single bilayer structure is not very efficient. Using multiple bilayers separated by insulating materials, on the other hand, results in the formation of dipoles in each layer that sum up to a total polarization (Figure 2). According to the Lambert−Beer law, however, each subsequent bilayer receives less light and therefore contributes less to total polarization. The LHC efficiency can be further improved by adding active layers of materials with absorbing band peaks at different wavelengths, from blue to infrared, aiming to explore multispectral absorption, covering a broad white light band such as that of the solar spectrum.

In their works on LHCs, Lanzani et al. present results on devices fabricated with molecular materials, such as copper phthalocyanine (CuPc) or metal-free phthalocyanine (H_2Pc) for donor, and buckminsterfullerene (C_{60}) or 3,4,9,10-perylenetetracarboxylic bisbenzimidazole (PTCBI) for acceptor.[9,13] These works provide experimental proof of concept of the functioning of LHCs as well as theoretical modeling of efficiency and the influence of different model parameters, indicating donor−acceptor layer thickness comparable to the singlet diffusion as one key property to obtain high device efficiencies. In addition, they present a very detailed multiscale model of OPV devices that describes the individual processes involved in the transformation of light into electrical current. The advanced complexity of the obtained set of equations, however, results in the necessity of numerical treatment. The obtained results were in good agreement to experimentally recorded transient current data, but due to the numerical description, lacks physical insights and prevents simple application to characterize many experimental curves. Although the LHC is interesting, not much has been done over the past decade since the first mention to explore the full potential of this device.

In this article, we present theoretical modeling and experimental results on fabrication and characterization of LHCs. In particular, we derive an analytical expression of the photogenerated transient current based on photophysical and electrodynamical principles, providing the opportunity to characterize experimental measurements in a simpler fashion. Furthermore, our experimental work focuses on polymer-based LHCs fabricated by layer-by-layer (LbL) assembly rather than small molecule devices obtained using thermal evaporation. The use of LbL allows the formation of many ultrathin layers with more uniform donor acceptor interfaces and hence improved formation of coherent dipoles, thus increasing significantly the photoinduced polarization $\mathcal{P}_p$ within the active layer. As illustrated in the right part of Figure 2, one can assume that the molecular acceptor tends to interpenetrate the polymeric-donor interface, e.g., due to diffusion processes, resulting in random orientation of generated dipoles which do not contribute to the total polarization of the LHC. To avoid this, the use of the polymeric acceptor promises less interpenetration and consequently a more efficient generation of coherent dipoles. Comparing the transient photocurrent between devices obtained using the same small molecule moieties as acceptor material, but one with the moieties as side groups of a cationic polyelectrolyte and the other with acceptors as free molecules, we demonstrate that all-polymer devices indeed yield more efficient LHCs, although generating less total charges due to reduced interface area. Finally, fitting our analytical model to the experimental transient currents not only showcases that our model is able to correctly describe the experimental results but also provides information about the processes inside the device, such as dipole lifetimes.

2. THEORY

Light Regime. Under illumination, the LHC builds up an internal polarization $\mathcal{P}_p$, due to photogenerated charges prevented from extraction by the insulating layers, inducing an output current through a load resistance that creates the external charges induced by $\mathcal{P}_p$ (Figure 1). The number $N(t)$ of photogenerated charges can be expressed as[14,15]

$$\frac{dN}{dt} = G_q - \frac{N}{\tau_q} \tag{1}$$

whose analytic solution, for G constant, is given by

https://doi.org/10.1021/acsapm.4c00751
ACS Appl. Polym. Mater. 2024, 6, 8040−8047

$$N = \tau_q G_q + (N_0 - \tau_q G_q)e^{-t/\tau_q} \quad (2)$$

Here, N represents the number of photogenerated charges Q with lifetime τ_q and generation rate G_q. In the case of very thin films, where the maximum charge separation is obtained nearly instantaneously, the number of photogenerated dipoles are approximately proportional to N, with generation rate $G_p \approx G_q$ (henceforth represented by G).

While the electrical displacement $\mathcal{D}$ of a charged capacitor relates to the external electric field $\mathcal{E}$ and polarization $\mathcal{P}$ by $\mathcal{D} = \epsilon_0\mathcal{E} + \mathcal{P} \equiv \epsilon\mathcal{E}$, the physical principle of an LHC has to include the additional amount $\mathcal{P}_p$ due to photopolarization, i.e.,

$$\mathcal{D} = \epsilon\mathcal{E} + \mathcal{P}_p \quad (3)$$

With this, the positive electric charge accumulated in the LHC top electrode is given by the integral over its surface

$$Q = \int_{top} \mathcal{D}\cdot\hat{\mathbf{n}}\,d^2r = \mathcal{D}A \quad (4)$$

where A is the capacitor plate area. The output voltage is given by the path integral inside the LHC between bottom and top electrodes

$$\mathcal{V} = -\int_{bot}^{top} \mathcal{E}\cdot\hat{\mathbf{r}}\,dr = \mathcal{E}\cdot d \quad (5)$$

where d is the LHC thickness. Combining eqs 3−5, it follows that

$$\mathcal{V}(t) = \frac{d}{\epsilon}\left(\frac{Q}{A} - \mathcal{P}_p\right) \quad (6)$$

where $\mathcal{P}_p = \mathcal{P}_p\cdot\hat{\mathbf{n}}$ is the strength of coherent photopolarization, i.e., the component of photopolarization in the direction perpendicular to the capacitor plates. Note that the lifetime τ_p of this coherent photopolarization is not necessarily equal to the lifetime of photogenerated charges τ_q because τ_p does not account for the contribution of noncoherent dipoles.

The coupling with a external load resistance R provides $\mathcal{V} + R\cdot i = 0$, where $i = dQ/dt$ is the output current. Using $C = \epsilon A/d$, eq 6 leads to

$$-R\cdot i = \frac{1}{C}(Q - A\cdot\mathcal{P}_p)$$

Differentiating with respect to time and rearranging the terms, it follows that

$$\frac{di}{dt} + \frac{i}{\tau_c} - \frac{A}{\tau_c}\frac{d\mathcal{P}_p}{dt} = 0 \quad (7)$$

where $\tau_c \equiv RC$ is the capacitor's charge/discharge characteristic time. Assuming that $\mathcal{P}_p$ dynamics is similar to that of charges in eq 1, with dipole lifetime τ_p, and inserting it into eq 7, gives

$$\frac{di}{dt} + \frac{i}{\tau_c} - \frac{A}{\tau_c}\left(G - \frac{\mathcal{P}_0}{\tau_p}\right)e^{-t/\tau_p} = 0$$

whose solution is given by

$$i(t) = \left(i_0 + \frac{\bar{i}}{\tau_c/\tau_p - 1}\right)e^{-t/\tau_c} - \left(\frac{\bar{i}}{\tau_c/\tau_p - 1}\right)e^{-t/\tau_p}, \quad (8)$$

where $\bar{i} \equiv A(G - \mathcal{P}_0/\tau_p)$ and $i(0) = i_0$.

Equation 8 shows how the extrinsic and intrinsic parameters, τ_c and τ_p, respectively, rule the rising and decay rate of the current peak upon illumination. Peak rising is dominated by e^{-t/τ_c} whenever $\tau_c/\tau_p < 1$, for which e^{-t/τ_p} dominates the decay rate. Otherwise, for $\tau_c/\tau_p > 1$ the situation is reversed. The output current due to illumination vanishes as the internal polarization reaches a saturation regime, except for large values of τ_c/τ_p, for which the output current is a longer process. In addition, the peak strength drops as τ_c/τ_p rises.

Dark Regime. If light is suddenly turned off after an interval Δt of illumination, then the photogeneration rate becomes $G = 0$, so that

$$\frac{d\mathcal{P}'_p}{dt'} = -\frac{\mathcal{P}'_p}{\tau_p} \quad (9)$$

where $\mathcal{P}'_p$ is the time-dependent dipole density in the LHC after light is off, i.e., for $t' = t - \Delta t$. Assuming that $\mathcal{P}'_p(0) = \mathcal{P}_p(\Delta t)$, the solution to eq 9 is

$$\mathcal{P}'_p = \mathcal{P}_p(\Delta t)e^{-t'/\tau_p} \quad (10)$$

From eqs 7 and 9, defining $\bar{i}' \equiv A\mathcal{P}_p(\Delta t)/\tau_p$, the output current i' after light is off will be given by

$$\frac{di'}{dt'} + \frac{i'}{\tau_c} + \frac{\bar{i}'}{\tau_c}\cdot e^{-t'/\tau_p} = 0$$

whose solution, assuming $i'(0) = i(\Delta t)$, is

$$i'(t') = \left(\frac{\bar{i}'}{\tau_c/\tau_p - 1}\right)e^{-t'/\tau_p} - \left(\frac{\bar{i}'}{\tau_c/\tau_p - 1} - i(\Delta t)\right)e^{-t'/\tau_c} \quad (11)$$

Equation 11 is similar to eq 8, but with inverted sign, which describes the reverse current due to internal charge recombination after light is turned off. This suggests that LHCs are candidates for current photogeneration applications where cyclic illumination takes place, with a period on the order of the larger between τ_p and τ_c.

Stacked LHC. In a multilayered or stacked LHC, as illustrated in Figure 2, additional active layers exploit the remaining light not absorbed by the first active layer and add their individual contribution to the output current. Assuming d as the average single LHC thickness and ϵ as the effective dielectric constant of the whole device, the output voltage then becomes

$$\mathcal{V}_n(t) = \sum_k^n \frac{d_k}{\epsilon_k}(\mathcal{D}_k - \mathcal{P}_{p,k}) = \frac{d}{\epsilon}\left(\frac{Q}{A} - \mathcal{P}_{p,n}\right)$$

where $\mathcal{P}_{p,n} = \sum_k^n \mathcal{P}_{p,k}$ is the total polarization. Assuming α as the effective absorption coefficient of the active layer and applying the Lambert−Beer formula, the generation rate at the k-th active layer is $G_k = G_0\cdot 10^{-k\alpha d}$, where G_0 is the generation rate at the first active layer. Therefore, assuming the same dynamic equation for each layer photopolarization $\mathcal{P}_k(t)$, eq 2 for photopolarization, and eq 10 for a stacked LHC with n active layers yield, respectively,

$$\mathcal{P}_{p,n} = \tau_p G_n + (\mathcal{P}_{0,n} - \tau_p G_n)e^{-t/\tau_p} \quad (12)$$

where $\mathcal{P}_{0,n} = \sum_k^n \mathcal{P}_{0,k}$ and $G_n = \sum_k^n G_k$, and

https://doi.org/10.1021/acsapm.4c00751
ACS Appl. Polym. Mater. 2024, 6, 8040−8047

$$\mathcal{P}'_{p,n} = \mathcal{P}_{p,n}(\Delta t)e^{-t'/\tau_p} \tag{13}$$

The similarity of eq 12 with eq 2 for photopolarization leads to the differential equation for the direct current output, i.e., under illumination, given by

$$\frac{di_n}{dt} + \frac{i_n}{\tau_c} - \frac{A}{\tau_c}\frac{d\mathcal{P}_{p,n}}{dt} = 0$$

which is similar to eq 8 and then its solution is

$$i_n(t) = \left(i_{0,n} + \frac{\overline{i}_n}{\tau_c/\tau_p - 1}\right)e^{-t/\tau_c} - \left(\frac{\overline{i}_n}{\tau_c/\tau_p - 1}\right)e^{-t/\tau_p} \tag{14}$$

where $i_{0,n} \equiv i_n(0)$ and $\overline{i}_n \equiv A(G_n - \mathcal{P}_{0,n}/\tau_p)$. Following the same reasoning, the reverse output current is

$$i'_n(t) = \left(\frac{\overline{i}'_n}{\tau_c/\tau_p - 1}\right)e^{-t/\tau_p} - \left(\frac{\overline{i}'_n}{\tau_c/\tau_p - 1}\right)e^{-t/\tau_c} \tag{15}$$

where $\overline{i}'_n \equiv A\mathcal{P}'_{0,n}$.

Equation 12 shows that the increase of output current with number of stacked active layers quickly reaches a limit due to light attenuation, since $G_n \to G_0/(1 - 10^{-\alpha d})$. Equations 14 and 15 show that another limitation for the contribution of additional active layers to the output current is the increase in τ_c due to the decrease in capacitance with thickness, i.e., $C_n = \epsilon A/nd$. Worth highlighting, computational analysis shows that multilayered LHC current reaches maximum $i/AG = 2$ for $\tau_c/\tau_p \to 0$.[16] The limiting number of stacked active layers depends on product αd.

3. MATERIALS AND FABRICATION

Indium tin oxide (ITO) contacts coated on glass were patterned by photolithography followed by cleaning and surface activation in potassium hydroxide (KOH)[17,18] prior to active layer deposition. Aiming to obtain multilayered LHC, LbL dip coating was chosen as the method of bottom-up nanofabrication.[19,20] For this, aqueous solutions of all of the polyelectrolytes were prepared at 0.5 mg/mL.

Purchased from Sigma-Aldrich, the polysalts poly(allylamine hydrochloride) (PAH), $M_W \sim 70{,}000$, and poly(sodium 4-styrenesulfonate) (PSS), $M_W \sim 1{,}000{,}000$ were selected, respectively, as cationic and anionic polyelectrolytes applied as the insulating layers, since they are nonconducting and transparent;[19,20] as donor and acceptor molecules, respectively, we selected poly(3-potassium-6-hexanoate thiophene) (P3KHT),[21] purchased from Rieke Metals Inc., and *N*,*N*′-bis(6-aminohexil)-3,4,9,10-perilenediimide (PDI-6N) or perylenediimide-functionalized polyethileneimine (PDI-PEI) (Figure 3), both synthesized in our laboratory.

The solubility of PDI-6N in water is granted by the side chains added chemically from 1,6-diaminohexane (DAH) to perylenediimide (PDI), which is water insoluble. PDI-6N is a small molecule, just like most of electron acceptor molecules.[22,23] However, as illustrated in Figure 2, a small molecule acceptor is able to interpenetrate the long chains of donor molecules in a random orientation that does not yield a coherent contribution to the nanodipoles in an LHC. In contrast, due to its long chain, the PDI-PEI macromolecule may significantly suppress such interpenetration.

PDI-6N [or PDI-PEI] was synthesized by the condensation of DAH [polyethylenimine (PEI)] with perylene-3,4,9,10-tetracarboxylic (PTCDA). A 10-fold equivalent was used in order to reduce the probability of cross-linking. Thus, 23 mmol of DAH [PEI, mer based], 2.3 mmol of PTCDA, 2.3 mmol of zinc acetate, and 10 g of imidazole were mixed in a round flask and heated for 6 h at 145 °C. The characteristic red color of PTCDA turned dark-brown [purple] as the reaction occurred. Imidazole was then removed from the reaction mixture by adding slightly acidic acetone. The remaining powder was suspended in water and filtered. In these conditions, PDI-6N [PDI-PEI] is soluble. The water solution was then neutralized and dried, providing solid PDI-6N [PDI-PEI] to be powdered.

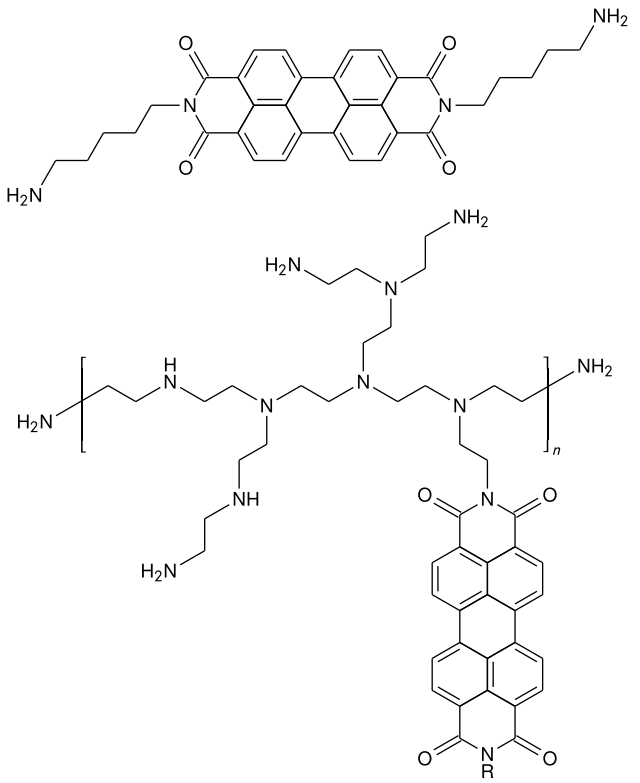

Figure 3. Planar chemical structures of PDI-6N (top) and PDI-PEI (bottom). The R stands for a radical or any possible chemical bond due to synthesis reaction.

For the LbL dip coating procedure, PAH, PSS, and P3KHT solutions were obtained by dissolving 5 mg of each solute in 10 mL of deionized water. To obtain the PDI-6N [PDI-PEI] solution, two drops of concentrated hydrochloric acid were added to a recipient containing 15 mg of PDI-6N [PDI-PEI] followed by an addition of 10 mL of deionized water. After both mechanical stirring and ultrasonic bath, another quantity of 10 mL of pure water was added to the solution for further dissolving. After more stirring, the solution was completed with water until reaching 30 mL.

Following LbL dip coating, 20 nm thick top metallic electrodes were deposited by high-vacuum vapor deposition of aluminum using a MBraum-evap 130. The final substrates consist of four separated LHC devices with an active area of 4.5 mm^2 each.

4. CHARACTERIZATION AND RESULTS

Absorption spectroscopy was performed using a Hitachi U2900 UV−vis spectrophotometer. Figure 4 shows the normalized absorption spectra for aqueous solutions of PDI-6N, PDI-PEI, and P3KHT in glass cuvette 1 mm thick (top) as well as absorbance for LHC devices with 30 active layers of PDI-6N/P3KHT and PDI-PEI/P3KHT, measured in an in-house sample holder sealed under inert atmosphere (bottom). The similarity of the red and black curves suggests that the optical band gap and electronic transitions for PDI-PEI is the same as that for PDI-6N, indicating that PEI yields no electronic change, working specifically as molecular orderer. Both LHC devices present a peak at 500 nm with shoulders at about 480 and 550 nm. Comparing to the normalized absorbance, these individual features can be attributed to the

https://doi.org/10.1021/acsapm.4c00751
ACS Appl. Polym. Mater. 2024, 6, 8040−8047

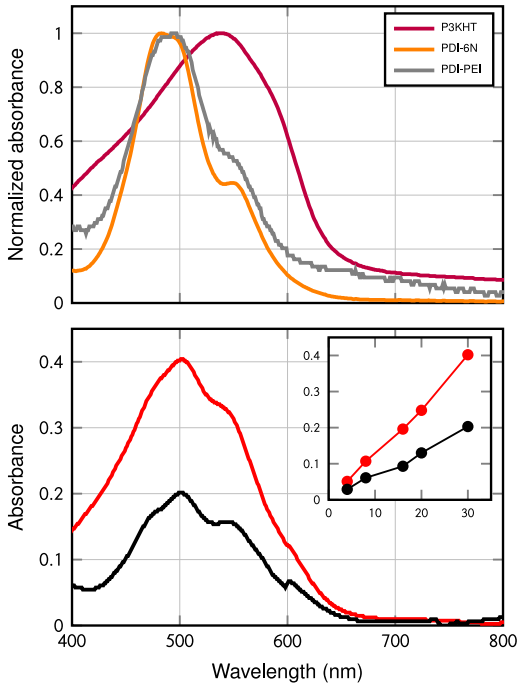

Figure 4. Top: Normalized absorbance for PDI-6N, PDI-PEI, and P3KHT aqueous solutions. **Bottom:** Absorbance spectrum of LHCs with 30 active layers made of PDI-6N/P3KHT (red) and PDI-PEI/P3KHT (black). **Inset:** Absorbance at 500 nm of LHCs for devices with 4, 8, 16, 20, and 30 active layers.

active layer materials. The 500 nm maximum and the 480 nm shoulder arise from the PDI moiety, whereas that near 550 nm is formed by both PDI and P3KHT. Following Lambert−Beer law, the linearly increasing trend of absorbance at 500 nm with the number of coated active layers suggests linear growth, as shown in the inset of Figure 4. By comparing the magnitudes, it is evident that the PDI-6N film absorbs about twice as much as the PDI-PEI, which means a higher generation of excitons in the small-molecule acceptor device. This difference can be related to the expected larger incorporation of PDI units due to less steric demand on the 6N side chains compared to PEI backbone.

Charge transfer from PDI to P3KHT was investigated by continuous-wave photoinduced absorption (cw-PA) spectroscopy and time-resolved transient absorption (TRTA).[24] A lock-in amplifier was used in the cw-PA setup for three measurements: the transmission spectra (T) of probe light mechanically modulated by a chopper, the change in transmission spectra (ΔT) caused by a digitally square modulated pump laser that overlapped with the probe spot, and the photoluminescence (PL) caused by the modulated pump laser with probe light turned off. Contribution of PL to ΔT was eliminated by subtraction before obtaining the normalized differential transmission $\Delta T/T$.

Figure 5 is the plot of the cw-PA spectra normalized by the absorbance $\mathcal{A}$ of the samples at pump wavelength, 488 nm, with pump modulation at 1 kHz, from which can be seen in-phase (P) and quadrature (Q) components. This normalization is important to account for the pumping photon conversion efficiency per molecular absorbing unit in the different samples, since the samples present different absorbance at pump wavelength. The P component displays positive photobleaching (PB) and negative photoabsorption

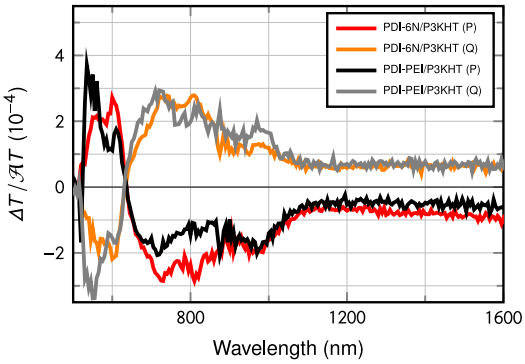

Figure 5. cw-PA spectra normalized to the absorbance $\mathcal{A}$(488nm) at pump wavelength of LHCs with 30 active layers based on PDI-6N/P3KHT and PDI-PEI/P3KHT after excitation at 488 nm with pump power at 25 mW and modulated at 1 kHz.

(PA) bands with a crossover at 640 nm. The PB band arises from the decrease in the absorbance of P3KHT caused by ground state depletion, while the PA band results from an increase in the absorption caused by the new optical transition states with respect to the originally neutral molecules as an indicative of photoinduced charge transfer from P3KHT to PDI. P and Q measurements are related to the charge generation, lifetime, and the pump modulation frequency.[25,14,26] Typically, the Q component is more sensitive to lifetime than P, so that the plot in Figure 5 indicates that the lifetime of photogenerated charges is practically the same for LHCs made of PDI-6N/P3KHT and PDI-PEI/P3KHT. The P magnitude of $\Delta T/\mathcal{A}T$ near 700 nm is about 1.5 times as large for PDI-6N/P3KHT as for PDI-PEI/P3KHT, suggesting that PDI-6N/P3KHT is quite more efficient in photogeneration of charges than PDI-PEI/P3KHT. This can be explained by the fact that PDI-6N units are smaller, closer together, and diffused into the P3KHT layer, providing larger contact surface area in comparison to PDI-PEI (Figure 2). Hence, the exciton-to-charge conversion efficiency is also higher in the small-molecule-acceptor-based device. As shown below, the benefit of using the PDI-PEI macromolecule as an acceptor in an LHC is that the transferred charges assume higher coherent orientation in order to generate higher output current.

This is confirmed in measurements of photocurrent performed by pumping at 488 nm with 10 mW 10 Hz square modulation and load resistance of 1 MΩ, as presented in Figure 6, where peak strength is three times larger for PDI-PEI/P3KHT than for PDI-6N/P3KHT. Data fitting with eq 14 provides the parameters presented in Table 1. The parameter $\bar{i}_n$, which indicates the generation rate of coherent dipoles (see definition below eq 14), is about 16 times larger for the PDI-PEI/P3KHT device than for that using PDI-6N/P3KHT, even with the absorbance of PDI-6N/P3KHT devices being about twice larger than that of PDI-PEI/P3KHT devices at the pump wavelength. This reinforces the hypothesis that macromolecule materials possess lower chances of interpenetration at the donor−acceptor interface, resulting in the improvement of the formation of coherent dipoles. In addition, τ_c is about five times larger for PDI-PEI/P3KHT LHC than for PDI-6N/P3KHT. As both devices were characterized at the same load resistance, this result suggests that the active layer based on PDI-PEI yields larger capacitance, probably due to the cross-linking polymer chain of PEI, which consists of many amine groups known to be very polar.[27−29] On the other hand, the

https://doi.org/10.1021/acsapm.4c00751
ACS Appl. Polym. Mater. 2024, 6, 8040−8047

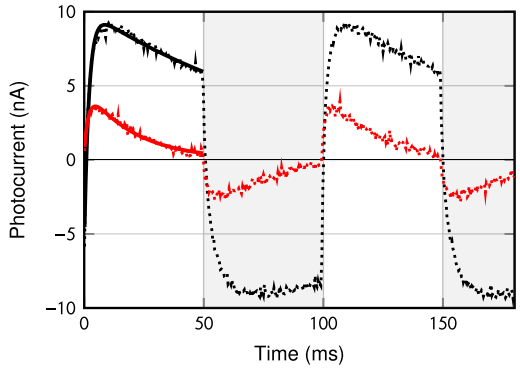

Figure 6. Dotted: Output current by LHCs based on PDI-6N/P3KHT (red) and PDI-PEI/P3KHT (black). The white area corresponds measurements under illumination, and the gray area, in dark. **Solid:** Fitting performed according to eqs 14 and 15.

Table 1. Fitting Parameters for the Plot in Figure 6 Using Eq 14

	PDI-6N/P3KHT	PDI-PEI/P3KHT
$i_{0,n}$ (nA)	0.552	−5.73
$\overline{i_n}$ (nA)	45.4	734
τ_c (ms)	20.7	92
τ_p (ms)	1.83	1.96

lifetime of dipoles τ_p differ by less than 10%, indicating that the different functionalizations of PDI do not affect the lifetime of dipoles, meaning that the electronic properties are due exclusively to the PDI units.

Aiming to assess the validity of our model, simultaneous measurements of photocurrent and TRTA spectroscopy were performed on a LHC made of PDI-PEI/P3KHT with 30 active layers. The same 488 nm continuous laser as for the cw-PA setup was utilized as a pump beam and illuminated the same device with a circular spot size of 6 mm. Due to the low sensitivity of the TRTA setup, pump power was raised to 25 mW for both TRTA and photocurrent measurements. Before hitting the sample, the light passes a beam splitter where the reflection is focused on a photodiode that acts as a trigger for a Tektronix TDS 320C oscilloscope. As a probe beam, an 890 nm laser diode was focused on the device, matching the pump laser spot. The reflection off the aluminum back electrode was then focused on a Thorlabs DET36A2 detector for the visible range and DET20C2 for the infrared, both with a built-in amplifier. Photocurrent results are shown in Figure 7 (top) along with respective theoretical curve fittings using eq 14 whose calculated parameters τ_c and τ_p are presented in Table 2.

As expected, the capacitor characteristic time depends on the load resistance and obeys the relation $\tau_c = RC$. On the other hand, the dipole lifetime seems to depend on the load resistance, probably due to the influence of the internal electric field in the LHC, which is strongly dependent on the external resistance. The lifetime of photogenerated charges τ_q can be estimated from measurements performed by TRTA, as plotted in Figure 7 (bottom) after the Savitzky−Golay filter for 51 successive points and third-order polynomial to clear noise. Its value after fitting with eq 2 for photogenerated charges is also presented in Table 2. As expected, the lifetime of the photogenerated charges is independent of the load resistance. They also do not depend on the modulation frequency, as it can be inferred from the TRTA data plotted in Figure 8

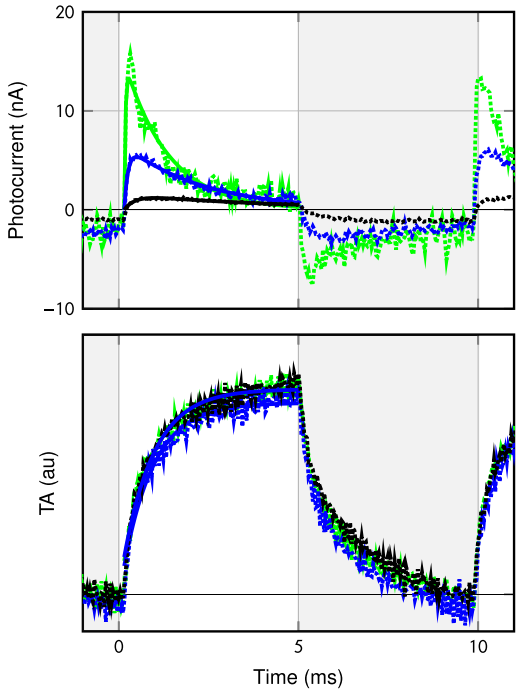

Figure 7. Photocurrent (top) and transient absorption (bottom) for external load resistors of 30 kΩ (green), 90 kΩ (blue), and 342 kΩ (black). Dotted lines represent the measured data, and solid lines result from theoretical fitting with eq 14 to the photocurrent or from monoexponential fitting to the transient absorption.

Table 2. Fitting Parameters Were Obtained from Eqs 2 and 14 for TRTA and Photocurrent Measurements, Respectively

	30 kΩ	90 kΩ	342 kΩ
τ_c (ms)	0.0356	0.108	0.302
τ_p (ms)	1.23	2.21	4.28
τ_q (ms)	0.816	0.848	0.855

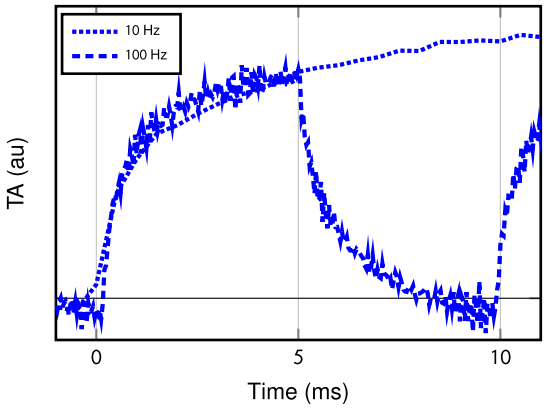

Figure 8. Comparison of transient absorption measurements for external load resistor of 90 kΩ with pump intensity of 25 mW at a frequency modulation of 10 and 100 Hz.

measured at different pump modulation frequencies under the same pump intensity and load resistance. The calculated charge lifetimes τ_q are on the same order of magnitude as those calculated for photopolarization. Its apparent lower value than τ_p might originate from the oversimplification in which the LbL layer thickness x is constant and the polarization $\mathcal{P}_p = exN$ is proportional to the photogeneration density N,

https://doi.org/10.1021/acsapm.4c00751
ACS Appl. Polym. Mater. 2024, 6, 8040−8047

so that $Ndx/dt \ll xdN/dt$. With this, although the monoexponential behavior generates good adjustment to the data, a more precise solution of the differential equation without oversimplification may lead to more precise data fitting.

5. CONCLUSIONS

Following the feasibility of fabrication of an LHC to provide output current leaded by photogeneration of nanodipoles, as first shown by Lanzani et al.,[9] a theory is developed analytically in this paper with photophysical ground, including device and circuit parameters, such as capacitance and load resistance. Furthermore, we fabricated LHCs based solely on polyelectrolyte LbL films and show here that a polymeric electron acceptor leads to improved final performance due to more ordered charge transfer that results in the higher polarization, even when providing less generation of charges compared to a small molecule. Correlating the results from the electrical characterization with those of the optical measurements shows that the lifetime of photogenerated charges is about 1 ms and does not depend on external parameters such as load resistance, light intensity, and modulation frequency, being in the same order of magnitude of photogenerated dipoles. On the other hand, the lifetime of photogenerated dipoles does depend on load resistance. We also show that the benefit of using the PDI-PEI as an acceptor in an LHC is that the charge transferred assumes an orientation with higher coherence in order to generate higher output current.

The conversion efficiency is calculated by dividing the output energy in the form of electrical current to the input energy in the form of light. The first one is the time integral of the load resistance times the output electrical current squared. The second one is the time integral of the light intensity times the light beam cross section area. Both theoretical and experimental analysis of efficiency is beyond the scope of this paper and is aimed to be presented in future work.

In the case discussed in this article, the light intensity can be considered a square function, for which the time integral is the intensity times area times the illumination time. Therefore, the efficiency increases with time until the external current reaches its peak and then decreases, tending to zero for a long illumination time. As a direct consequence, long lasting illumination leads to low efficiency output of an LHC. Aiming to test the validity of the developed theory, the pumping modulation periods used to the characterizations in this work were very long in comparison to the photogenerated charges lifetime. Although the device efficiency is far from a practical power source, this work presents an advance on the nanoscale of its fabrication with a strategy to reduce interpenetration among layers that significantly improves their performance. These results indicate that this organic device is open to further improvement.

AUTHOR INFORMATION

Corresponding Author

Joaquim B. de Lima Filho − *São Carlos Institute of Physics, University of São Paulo, São Carlos, Brazil 13 566-590; Instituto Federal de Educação, Ciência e Tecnologia do Ceará, Crateús, Brazil 63 708-260;* orcid.org/0000-0003-2452-6579; Email: joaquim.brasil@gmail.com

Authors

Florian Günther − *São Carlos Institute of Physics, University of São Paulo, São Carlos, Brazil 13 566-590; Instituto de Geociências e Ciências Exatas, Universidade Estadual Paulista, Rio Claro, Brazil 13 506-900;* orcid.org/0000-0001-5002-4172

Bruno Bassi Millan Torres − *São Carlos Institute of Physics, University of São Paulo, São Carlos, Brazil 13 566-590;* orcid.org/0000-0001-5999-6488

Paulo B. Miranda − *São Carlos Institute of Physics, University of São Paulo, São Carlos, Brazil 13 566-590;* orcid.org/0000-0002-2890-0268

Complete contact information is available at: https://pubs.acs.org/10.1021/acsapm.4c00751

Funding

The Article Processing Charge for the publication of this research was funded by the Coordination for the Improvement of Higher Education Personnel - CAPES (ROR identifier: 00x0ma614).

Notes

The authors declare no competing financial interest.

ACKNOWLEDGMENTS

The authors acknowledge São Carlos Institute of Physics (IFSC) and University of São Paulo (USP) for providing infrastructure. We also acknowledge Coordenação de Aperfeiçoamento de Pessoal de Nível Superior (CAPES) (Finance Code 001), Fundação de Amparo à Pesquisa do Estado de São Paulo (FAPESP) (2018/15670-5), Conselho Nacional de Desenvolvimento Científico e Tecnológico (CNPq) (442239/2017-3 and 3155772/2020-4), and Instituto Nacional de Ciência e Tecnologia em Eletrônica Orgânica (INEO) (CNPq/FAPESP: 2008/57706-4) for providing financial support.

REFERENCES

(1) Lu, L.; Kelly, M. A.; You, W.; Yu, L. Status and prospects for ternary organic photovoltaics. *Nat. Photonics* **2015**, *9* (8), 491−500.

(2) Lin, Y.; Zhan, X. Oligomer molecules for efficient organic photovoltaics. *Accounts of chemical research* **2016**, *49* (2), 175−183.

(3) Lee, H.; Park, C.; Sin, D. H.; Park, J. H.; Cho, K. Recent advances in morphology optimization for organic photovoltaics. *Adv. Mater.* **2018**, *30* (34), 1800453.

(4) Cheng, P.; Li, G.; Zhan, X.; Yang, Y. Next-generation organic photovoltaics based on non-fullerene acceptors. *Nat. Photonics* **2018**, *12* (3), 131−142.

(5) Lechene, B. P.; Cowell, M.; Pierre, A.; Evans, J. W.; Wright, P. K.; Arias, A. C. Organic solar cells and fully printed super-capacitors optimized for indoor light energy harvesting. *Nano Energy* **2016**, *26*, 631−640.

(6) Zhang, Y.; Samuel, I. D. W.; Wang, T.; Lidzey, D. G. Current status of outdoor lifetime testing of organic photovoltaics. *Advanced Science* **2018**, *5* (8), 1800434.

(7) Yuan, J.; Huang, T.; Cheng, P.; Zou, Y.; Zhang, H.; Yang, J. L.; Chang, S.-Y.; Zhang, Z.; Huang, W.; Wang, R.; Meng, D.; Gao, F.; Yang, Y. Enabling low voltage losses and high photocurrent in fullerene-free organic photovoltaics. *Nat. Commun.* **2019**, *10* (1), 570.

(8) Hahn, T.; Tscheuschner, S.; Kahle, F.-J.; Reichenberger, M.; Athanasopoulos, S.; Saller, C.; Bazan, G. C.; Nguyen, T.-Q.; Strohriegl, P.; Bassler, H.; Kohler, A. Monomolecular and bimolecular recombination of electron−hole pairs at the interface of a bilayer organic solar cell. *Adv. Funct. Mater.* **2017**, *27* (1), 1604906.

(9) Garbugli, M.; Porro, M.; Roiati, V.; Rizzo, A.; Gigli, G.; Petrozza, A.; Lanzani, G. Light energy harvesting with nano-dipoles. *Nanoscale* **2012**, *4* (5), 1728−1733.
(10) Zhu, X.-Y.; Yang, Q.; Muntwiler, M. Charge-transfer excitons at organic semiconductor surfaces and interfaces. *Accounts of chemical research* **2009**, *42* (11), 1779−1787.
(11) Mikhnenko, O. V.; Blom, P. W. M.; Nguyen, T.-Q. Exciton diffusion in organic semiconductors. *Energy Environ. Sci.* **2015**, *8* (7), 1867−1888.
(12) Kumar, P.; Jain, S. C.; Kumar, H.; Chand, S.; Kumar, V. Effect of illumination intensity and temperature on open circuit voltage in organic solar cells. *Appl. Phys. Lett.* **2009**, *94* (18), 183505.
(13) Porro, M.; de Falco, C.; Verri, M.; Lanzani, G.; Sacco, R. Multiscale simulation of organic heterojunction light harvesting devices. *COMPEL: The International Journal for Computation and Mathematics in Electrical and Electronic Engineering* **2014**, *33* (4), 1107−1122.
(14) Epshtein, O.; Nakhmanovich, G.; Eichen, Y.; Ehrenfreund, E. Dispersive dynamics of photoexcitations in conjugated polymers measured by photomodulation spectroscopy. *Phys. Rev. B* **2001**, *63* (12), 125206.
(15) Epshtein, O.; Eichen, Y.; Ehrenfreund, E.; Wohlgenannt, M.; Vardeny, Z. V. Linear and nonlinear photoexcitation dynamics in π-conjugated polymers. *Physical review letters* **2003**, *90* (4), No. 046804.
(16) de Lima Filho, J. B. Optoelectronic characterization of organic photovoltaic devices with emerging achitectures. *PhD thesis*. Universidade de São Paulo: São Carlos, 2020.
(17) Cras, J. J.; ROWE-TAITT, C. A.; Nivens, D. A.; Ligler, F. S. Comparison of chemical cleaning methods of glass in preparation for silanization. *Biosens. Bioelectron.* **1999**, *14*, 683−688.
(18) Swain, G. M. Solid electrode materials. pretreatment and activation. In *Handbook of electrochemistry*; Zoski, C. G., Ed.; Elsevier: Amsterdam, 2007.
(19) Ariga, K.; Hill, J. P.; Ji, Q. Layer-by-layer assembly as a versatile bottom-up nanofabrication technique for exploratory research and realistic application. *Phys. Chem. Chem. Phys.* **2007**, *9* (19), 2319−2340.
(20) Elosua, C.; Lopez-Torres, D.; Hernaez, M.; Matias, I. R; Arregui, F. J Comparative study of layer-by-layer deposition techniques for poly (sodium phosphate) and poly (allylamine hydrochloride). *Nanoscale Res. Lett.* **2013**, *8*, 539.
(21) Vikulina, A. S.; Anissimov, Y. G.; Singh, P.; Prokopovic, V. Z.; Uhlig, K.; Jaeger, M. S.; von Klitzing, R.; Duschl, C.; Volodkin, D. Temperature effect on the build-up of exponentially growing polyelectrolyte multilayers. An exponential-to-linear transition point. *Phys. Chem. Chem. Phys.* **2016**, *18* (11), 7866−7874.
(22) Demeter, D.; Rousseau, T.; Leriche, P.; Cauchy, T.; Po, R.; Roncali, J. Manipulation of the Open-Circuit Voltage of Organic Solar Cells by Desymmetrization of the Structure of Acceptor− Donor− Acceptor Molecules. *Adv. Funct. Mater.* **2011**, *21* (22), 4379−4387.
(23) Zhang, G.; Zhao, J.; Chow, P. C. Y.; Jiang, K.; Zhang, J.; Zhu, Z.; Zhang, J.; Huang, F.; Yan, H. Nonfullerene acceptor molecules for bulk heterojunction organic solar cells. *Chem. Rev.* **2018**, *118* (7), 3447−3507.
(24) Menke, S. M.; Holmes, R. J. Exciton diffusion in organic photovoltaic cells. *Energy Environ. Sci.* **2014**, *7* (2), 499−512.
(25) Kobayashi, T.; Kinoshita, K.; Nagase, T.; Naito, H. Continuous-wave photoinduced absorption studies in polythiophene and fullerene blended thin films. *Phys. Rev. B* **2011**, *83* (3), No. 035305.
(26) Cole, K. S.; Cole, R. H. Dispersion and Absorption in Dielectrics I. Alternating Current Characteristics. *J. Chem. Phys.* **1941**, *9* (4), 341−351.
(27) Abdollahi, A.; Dashti, A. Photosensing of chain polarity and visualization of latent fingerprints by amine- functionalized polymer nanoparticles containing oxazolidine. *Eur. Polym. J.* **2023**, *191*, 112038.
(28) Lee, B. R.; Jung, E. D.; Nam, Y. S.; Jung, M.; Park, J. S.; Lee, S.; Choi, H.; Ko, S.-J.; Shin, N. R.; Kim, Y.-K.; Kim, S. O.; Kim, J. Y.; Shin, H.-J.; Cho, S.; Song, M. H. Amine-based polar solvent treatment for highly efficient inverted polymer solar cells. *Advanced materials* **2014**, *26* (3), 494−500.
(29) Erdem, S. S.; Karahan, O.; Yıldız, I.; Yelekci, K. A computational study on the amine-oxidation mechanism of monoamine oxidase: Insight into the polar nucleophilic mechanism. *Organic & biomolecular chemistry* **2006**, *4* (4), 646−658.

https://doi.org/10.1021/acsapm.4c00751
ACS Appl. Polym. Mater. 2024, 6, 8040−8047